A *Lotus japonicus* cytoplasmic kinase connects Nod factor perception by the NFR5 LysM receptor to nodulation

Jaslyn E. M. M. Wong[a,1,2], Marcin Nadzieja[a,1], Lene H. Madsen[a], Christoph A. Bücherl[b], Svend Dam[a], Niels N. Sandal[a], Daniel Couto[b,3], Paul Derbyshire[b], Mette Uldum-Berentsen[a], Sina Schroeder[a,4], Veit Schwämmle[c], Fábio C. S. Nogueira[d], Mette H. Asmussen[a], Søren Thirup[a], Simona Radutoiu[a], Mickaël Blaise[a,5], Kasper R. Andersen[a], Frank L. H. Menke[b], Cyril Zipfel[b,6], and Jens Stougaard[a,7]

[a]Department of Molecular Biology and Genetics, Aarhus University, DK-8000 Aarhus, Denmark; [b]The Sainsbury Laboratory, University of East Anglia, Norwich NR4 7UH, United Kingdom; [c]Department of Biochemistry and Molecular Biology, University of Southern Denmark, DK-5230 Odense, Denmark; and [d]Proteomics Unit, Chemistry Institute, Federal University of Rio de Janeiro, 21941-909, Rio de Janeiro, Brazil

Edited by David C. Baulcombe, University of Cambridge, Cambridge, United Kingdom, and approved June 4, 2019 (received for review September 7, 2018)

The establishment of nitrogen-fixing root nodules in legume–rhizobia symbiosis requires an intricate communication between the host plant and its symbiont. We are, however, limited in our understanding of the symbiosis signaling process. In particular, how membrane-localized receptors of legumes activate signal transduction following perception of rhizobial signaling molecules has mostly remained elusive. To address this, we performed a coimmunoprecipitation-based proteomics screen to identify proteins associated with Nod factor receptor 5 (NFR5) in *Lotus japonicus*. Out of 51 NFR5-associated proteins, we focused on a receptor-like cytoplasmic kinase (RLCK), which we named NFR5-interacting cytoplasmic kinase 4 (NiCK4). NiCK4 associates with heterologously expressed NFR5 in *Nicotiana benthamiana*, and directly binds and phosphorylates the cytoplasmic domains of NFR5 and NFR1 in vitro. At the cellular level, *Nick4* is coexpressed with *Nfr5* in root hairs and nodule cells, and the NiCK4 protein relocates to the nucleus in an NFR5/NFR1-dependent manner upon Nod factor treatment. Phenotyping of retrotransposon insertion mutants revealed that NiCK4 promotes nodule organogenesis. Together, these results suggest that the identified RLCK, NiCK4, acts as a component of the Nod factor signaling pathway downstream of NFR5.

NFR5 | NiCK4 | RLCK | *Lotus* | nodulation

Legumes and rhizobia initiate symbiosis by exchanging signal molecules in a bidirectional communication, which ultimately leads to the formation of nitrogen-fixing root nodules in the host plant (1, 2). Flavones or isoflavones secreted into the rhizosphere by legume plants associate with the rhizobial NodD protein that activates a set of genes synthesizing lipo-chitooligosaccharides called Nod factor (NF) (3). In turn, these rhizobial NFs are perceived by LysM-type receptors that trigger nodule organogenesis and infection thread formation (4). In *Lotus japonicus*, dedicated plasma membrane (PM)-localized receptors—NFR1, NFR5, and NFRe (5–7)—perceive NFs that constitute the major rhizobial signal (8–11). Both NFR1 and NFR5 are indispensable for NF signaling (5, 6) while NFRe was suggested to amplify signaling in root epidermal cells (7). NFR1, NFR5, and NFRe are lysin motif (LysM) receptor kinases (RKs) composed of 3 LysM domains in the extracellular region, a single-pass transmembrane domain, and an intracellular kinase domain. Purified NFR1, NFR5, and NFRe can directly and independently bind NF through their extracellular domains (7, 12). The kinase domains of NFR1 and NFRe are active in vitro (7, 13). However, the pseudokinase domain of NFR5 has a truncated activation loop, an altered DFG motif, lacks an APE motif, and is inactive in vitro (12, 13).

The earliest responses of NF from *Mesorhizobium loti* that nodulates *L. japonicus* include depolarization of the PM and alkalization of root hair extracellular space (6, 14, 15). Application of NF in nanomolar concentrations also results in calcium influx and perinuclear calcium oscillations (16–18). Shortly after *M. loti* inoculation, root hair deformation and curling responses occur (6). In later stages of the developmental process, infection threads are formed and nodule primordia develop in the root cortex (6, 19, 20).

Single *nfr1* or *nfr5* mutants are unresponsive to *M. loti* and NF treatments (5, 6). This phenotypic similarity suggests that NFR1 and NFR5 may be part of the same signaling complex. Several lines of evidence support this notion. First, NFR1 associates with NFR5 in bimolecular fluorescence complementation

Significance

Legume receptors perceive Nod factor signal molecules at the plasma membrane of epidermal cells and initiate a signal transduction process that leads to the development of root nodules that house nitrogen-fixing rhizobia. Nodule organs are formed by reinitiation of cell divisions in already differentiated root cells. Previous genetic screens have identified plant genes involved in nodulation; however, the receptor-triggered relay mechanism activating the developmental program in the nucleus is still unknown. We present a proteomics approach that identified proteins that associate with the *Lotus japonicus* Nod factor receptor 5 (NFR5), among which the NFR5-interacting cytoplasmic kinase 4 (NiCK4) appears to be an important link between Nod factor perception by NFR5 and nodule organogenesis.

Author contributions: J.E.M.M.W., M.N., D.C., C.Z., and J.S. designed research; J.E.M.M.W., M.N., L.H.M., C.A.B., S.D., N.N.S., P.D., M.U.-B., S.S., V.S., F.C.S.N., M.H.A., and F.L.H.M. performed research; S.T., S.R., M.B., and K.R.A. contributed new reagents/analytic tools; J.E.M.M.W., M.N., S.D., D.C., V.S., F.C.S.N., and F.L.H.M. analyzed data; and J.E.M.M.W. and J.S. wrote the paper.

The authors declare no conflict of interest.

This article is a PNAS Direct Submission.

[1]J.E.M.M.W. and M.N. contributed equally to this work.

[2]Present address: Medical Research Council Laboratory of Molecular Biology, Cambridge CB2 0QH, United Kingdom.

[3]Present address: Structural Plant Biology Laboratory, Department of Botany and Plant Biology, University of Geneva, 1211 Geneva, Switzerland.

[4]Present address: Faculty of Biology, University of Freiburg, 79104 Freiburg, Germany.

[5]Present address: Institut de Recherche en Infectiologie de Montpellier, CNRS, UMR 9004, Université de Montpellier, 34293 Montpellier Cedex 5, France.

[6]Present address: Institute of Plant and Microbial Biology and Zurich–Basel Plant Science Center, University of Zurich, 8008 Zurich, Switzerland.

[7]To whom correspondence may be addressed. Email: stougaard@mbg.au.dk.

This article contains supporting information online at www.pnas.org/lookup/suppl/doi:10.1073/pnas.1815425116/-/DCSupplemental.

Published online June 25, 2019.

(BiFC) experiments using *Nicotiana benthamiana* leaves (13). In the BiFC assays, cell death responses were observed when NFR5 was coexpressed with wild-type NFR1 but not the T483A kinase-dead variant of NFR1 (13). Second, spontaneous nodulation that occurs upon overexpression of *Nfr5* in *L. japonicus* transformed roots was not observed in an *nfr1* mutant background (21). Finally, the extension of the host range of *Medicago truncatula* (*Mt*) to include *M. loti* requires the transfer of both *Nfr1* and *Nfr5* (22).

Genetic approaches have identified several symbiosis components acting downstream of NFR1 and NFR5. A putative coreceptor is the symbiosis receptor kinase (SymRK), which associates with NFR1 or NFR5 upon overexpression in *N. benthamiana* leaves and transformed *L. japonicus* root systems (21). SymRK (23, 24), nucleoporins NUP85 (25), NUP133 (26), and NENA (27), potassium channels Castor and Pollux (28–30), and calcium channels of the CNGC15 family (31) all act upstream of NF-induced perinuclear calcium oscillations. The calcium signature generated is then decoded by the calcium/calmodulin-dependent kinase (CCaMK) (32–34) and the CYCLOPS transcription factor (35, 36) that resides in the nucleus. This triggers the expression and activation of additional transcription factors such as *Nin*, *Nsp1*, *Nsp2*, *Ern1*, and *NF-Y*s (35–45) that regulate genes required for nodule formation and function.

The mechanisms of the early steps of this pathway connecting ligand perception by NF receptors at the PM to downstream signaling components are missing. An explanation for this paucity of interacting components and secondary signal molecules could be gene redundancy or functional compensation preventing their identification using molecular genetic approaches. Recent development in coimmunoprecipitation (co-IP) and proteomics technologies have led to the identification of interactors of plant RKs and receptor-like proteins (46, 47). Here, we present a proteomics approach in which proteins associated with enhanced yellow fluorescent protein (eYFP)- and HA-tagged NFR5 (NFR5-eYFP-HA) in *L. japonicus* were isolated in co-IP experiments and identified by mass spectrometry (MS). One of the NFR5-associated proteins, which we named NFR5-interacting cytoplasmic kinase 4 (NiCK4), was characterized biochemically and genetically. The discovery of NiCK4 as a signaling component that links NF perception at the PM to downstream nodulation signaling indicates that an intricate phosphorylation cascade mechanism involving the NFR5 pseudokinase activates the signal transduction process.

Results

Identification of NFR5-Associated Proteins. To identify components of the NFR5 signaling pathway, we generated *L. japonicus* transgenic plants expressing NFR5-eYFP-HA (hereafter referred to as NFR5-eYFP) to perform co-IP experiments. We first assessed that the NFR5-eYFP construct was capable of rescuing the *nfr5-2* nonnodulating phenotype (*SI Appendix*, Fig. S1*A*) before generating *p35S:Nfr5-eYFP* lines. In epidermal root cells and root hairs, NFR5-eYFP localized predominantly to the cell periphery and mobile endomembrane compartments including the endoplasmic reticulum (*SI Appendix*, Fig. S1*B*). NF treatments also produced the expected root hair deformations (*SI Appendix*, Fig. S1*C*), thus attesting to the responsiveness of our transgenic lines. We then carried out large-scale triplicate co-IP experiments using ∼3,000 NFR5-eYFP roots for each of the triplicate experiments, as summarized in *SI Appendix*, Fig. S1*D*. The transgenic roots were treated either with 200 nM purified *M. loti* NF or water (mock) for 15 min. Nontreated wild-type Gifu roots were used as a specificity control.

NFR5-eYFP was successfully captured on GFP-trap beads (Fig. 1*A*) and was identified with 78% coverage by MS (*SI Appendix*, Fig. S2*A*). Remarkably, we discovered 2 in vivo phosphorylation sites, S574 and T576 (*SI Appendix*, Fig. S2 *C* and *D*), in addition to S282 (*SI Appendix*, Fig. S2*B*), which was previously shown to be phosphorylated by NFR1 and SymRK (13). This suggests that NFR5 may be phosphorylated by hitherto-unknown components (*SI Appendix*, Fig. S2 *B–D*). We defined NFR5-associated proteins as those that are represented by at least 2 unique peptides (with Mascot ion scores above 20) in all 3 biological replicates (*SI Appendix*, Table S1) while absent from the list of unspecific proteins (*SI Appendix*, Table S2). Two hundred and fifteen putative NFR5-associated proteins, represented by over 2,000 peptide spectra, fulfilled these criteria (*SI Appendix*, Table S1).

Two hundred and nine proteins that were present in both mock- and NF-treated samples were ranked according to spectral count (*SI Appendix*, Table S1). The remaining 6 NFR5-associated proteins that were either enriched in NF- or mock-treated samples were placed at the bottom of the list (*SI Appendix*, Table S1) and were ranked 210–213, and 214 and 215, respectively. We further

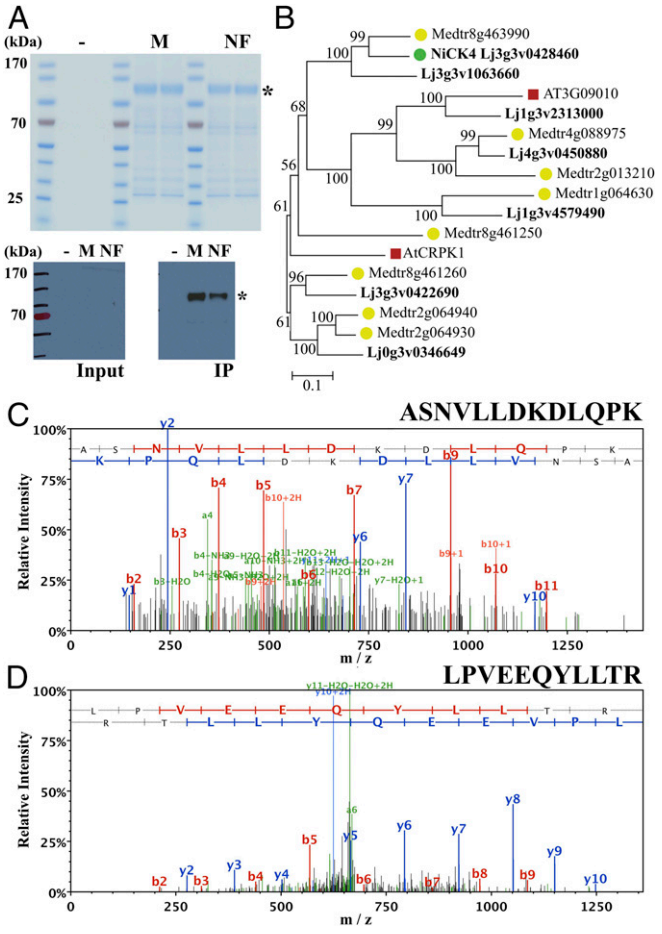

Fig. 1. Co-IP of NFR5-eYFP and MS discovery of NiCK4. (*A*) SimplyBlue SafeStained gel of proteins coimmunoprecipitated with GFP-trap beads. The molecular weights of the marker proteins (in kilodaltons) are indicated next to their corresponding protein bands. The corresponding Western blot of crude extract (input) and coimmunoprecipitated NFR5-eYFP proteins with anti–GFP-HRP antibodies used for visualization. (–) indicates the nontreated WT Gifu root sample, while (M) and (NF) indicate mock- and NF-treated NFR5-eYFP–expressing root samples, respectively. The asterisks indicate the positions of NFR5-eYFP. Three biological replicates were prepared for each condition. (*B*) Phylogenetic tree of *L. japonicus*, *M. truncatula*, and *A. thaliana* members in the CRPK1 family. NiCK4 is indicated with a green filled circle, and *M. truncatula* and *A. thaliana* RLCKs are indicated with filled yellow circles or red squares, respectively. The phylogenetic tree was constructed with the CLC main workbench using the neighbor joining method and Jukes–Cantor protein distance measurement with 10,000 bootstrap replicates (https://www.qiagenbioinformatics.com). (*C* and *D*) Two representative mass spectra of 2 unique peptides of NiCK4, ASNVLLDKDLQPK (*C*) and LPVEEQYLLTR (*D*), identified in mock-treated samples, with Mascot ion scores of 49.8 and 47.2, respectively.

filtered our candidate list by removing highly abundant and related proteins by comparison with previously published proteomics data (48) and additional data generated from liquid chromatography–mass spectrometry (LC-MS) proteomics studies of *L. japonicus* roots (*SI Appendix*, Table S3 and *Materials and Methods*) to reach a reduced set of 51 root-hair–expressed NFR5-associated proteins (Table 1) represented by 246 unique peptides (*SI Appendix*, Table S4). This includes high-interest signaling candidates such as receptor kinases, receptor-like cytoplasmic kinases (RLCKs), phosphatases, as well as cell wall remodeling proteins (Table 1).

NiCK4 Is an RLCK that Could Relay Signals Downstream of NFR5. RLCKs are pivotal in linking ligand perception of PM-localized pattern recognition receptors to downstream components (49–59). The fourth NFR5-associated RLCK, which we have renamed NiCK4 for NFR5-interacting cytoplasmic kinase 4, was therefore selected for further in vivo and in vitro investigations regarding a possible role in symbiosis signaling and to assess the validity and accuracy of our IP-MS approach. NiCK4 was selected over the other 3 RLCKs because we were interested in identifying a dynamic protein component that could potentially link NF perception at the PM to nuclear events that lead to nodulation. NiCK4 is a prime candidate as the closest *Arabidopsis thaliana* (*At*) homolog of NiCK4 is CRPK1 (AT1G16670) (Fig. 1*B* and *SI Appendix*, Fig. S4), which is involved in transducing cold signal from the PM to the nucleus through phosphorylation of 14-3-3 proteins (58). Another interesting observation is that the number of *L. japonicus* and *M. truncatula* RLCKs in the CRPK1 family is 7 and 8, respectively, compared with 2 in *A. thaliana* (Fig. 1*B* and *SI Appendix*, Fig. S4). As *L. japonicus* and *M. truncatula* have the capacity to establish symbiotic relationships with rhizobia and arbuscular mycorrhiza fungi, one is tempted to speculate that some of these RLCK paralogs may have been neofunctionalized to serve symbiotic functions. Finally, gene expression analyses of the 4 NFR5-associated RLCKs available in the *Lotus* Base (60, 61) revealed that the expression of *Nick4* is the lowest among the 4 RLCKs in *L. japonicus* root hairs (*SI Appendix*, Fig. S5) (61). The detection of NiCK4 in 3 independent co-IP experiment, despite relatively low gene expression, therefore suggests that the association of NiCK4 and NFR5 is robust. Two spectra representing unique peptides of NiCK4 are shown in Fig. 1 *C* and *D*.

NiCK4 Localizes to the PM and Directly Interacts with NFR5. A prerequisite for complex formation is that NiCK4 and NFR5 should both be found at the same subcellular location. To assess this, NiCK4-mCherry and NFR5-eGFP fusion proteins were overexpressed in *N. benthamiana* leaves for localization studies. As a control, eGFP was N-terminally fused to *L. japonicus* low-temperature–induced protein 6B (*Lj*LTI6b) PM marker (62). Our results indicate that individually expressed NiCK4-mCherry, NFR5-eGFP, and eGFP-*Lj*LTI6b or coexpressed NiCK4 and NFR5-eGFP or eGFP-*Lj*LTI6b all localize at the PM of leaf epidermal cells, as confirmed by plasmolysis (*SI Appendix*, Figs. S6 and S7). The PM localization of NiCK4-eGFP was further confirmed in *Lotus* roots (*SI Appendix*, Fig. S8). Despite being a predicted cytoplasmic protein with no transmembrane domains, the PM localization of NiCK4 may be explained by interactions with PM-bound RKs or via lipid-anchoring posttranslational modifications. Fluorescence resonance energy transfer (FRET) measurements by acceptor photobleaching revealed that NiCK4-mCherry interacts with NFR5-eGFP (Fig. 2*A*) but not eGFP-*Lj*LTI6b in *N. benthamiana* (Fig. 2*B*).

Upon verifying that NiCK4 and NFR5 both localize to the PM, reciprocal co-IP experiments were performed using NiCK4-FLAG as a bait to validate the interaction between NiCK4 and NFR5. Anti-FLAG pulldown experiments were performed using NiCK4-FLAG, eGFP-*Lj*LTI6b, and NFR5-eGFP fusion proteins that were expressed in *N. benthamiana* leaves. NiCK4-FLAG was successfully enriched in coimmunoprecipitated samples (IP) as detected on Western blots with anti-FLAG antibodies (Fig. 2*C*). The eGFP-*Lj*LTI6b PM marker and NFR5-eGFP were well detected in the crude lysate (input) when expressed individually or when coexpressed with NiCK4-FLAG (Fig. 2*C*). However,

Table 1. Filtered list of 51 putative NFR5-associated proteins

No.	Protein
Receptor kinases	
1	AtCRK29-like protein
2	AT2G23200-like CrRLK1L protein
3	AtBIR1-like protein 1
4	AtRLK7-like protein
5	AtPERK1-like protein
6	LjCERK6 LysM protein
7	AtHERK1-like CrRLK1L protein
8	AtBIR1-like protein 2
9	LjLYS13 LysM protein
Receptor-like cytoplasmic kinases	
10	AtPTI1-like protein
11	MtSPK1-like protein
12	AtBSK8-like protein
13	NiCK4/AtCRPK1-like protein
Phosphatases	
14	Phosphoinositide phosphatase/AtRHD4-like protein
15	AtPP2C76-like protein
16	PP6 regulatory subunit/AtSAL1-like protein
17	PP2A B″β regulatory subunit-like protein
18	LjLNP2
Cell wall remodeling proteins	
19	Putative pectinacetylesterase
20	Putative *O*-fucosyltransferase
21	Putative callose synthase/AtGSL5-like protein
22	Putative callose synthase/AtGLS10-like protein
23	LjPLENTY2/Hyp *O*-arabinosyltransferase
24	Putative xyloglucan xylosyltransferase
25	AtCesA2-like protein
26	Putative galacturonosyltransferase
27	AtCesA3-like protein
Ion pumps	
28	AtAHA2-like PM proton pump
29	AtMIA-like protein
30	MtMCA8-like ER calcium pump
31	AtACA10-like PM calcium pump
Others	
32	AtAIR9-like protein
33	Putative E3 ubiquitin-protein ligase
34	12X transmembrane protein
35	ER membrane protein complex subunit-like protein 1
36	DUF1682-containing protein
37	AtDaysleeper-like protein
38	AtUXT3-like protein
39	AtRFC3-like protein
40	AtERD4-like protein
41	Putative carboxypeptidase
42	FG-GAP repeat-containing protein
43	MtHMGR1-like protein
44	PI4K-alpha-like protein
45	Calcium-dependent lipid-binding protein
46	AtTMPIT-like protein
47	ER membrane protein complex subunit-like protein 2
48	Putative calmodulin-binding transcription activator 2
49	AtSMC1-like protein
50	Paladin-like protein
51	Uncharacterized protein

Some proteins were named based on homologs identified in *A. thaliana* (*At*) or *M. truncatula* (*Mt*). NFR5-associated proteins that were NF- or mock-enriched are indicated in green or red, respectively.

only NFR5-eGFP and not eGFP-*Lj*LTI6b coimmunoprecipitated with NiCK4-FLAG (Fig. 2*C*). In addition, no unspecific binding of NFR5e-GFP to anti-FLAG beads coated with synthetic FLAG peptides was observed (Fig. 2*C*, lane 5). Altogether, our results indicate that the interaction of NFR5-eGFP and NiCK4-FLAG was not due to nonspecific contributions from the GFP or FLAG tags.

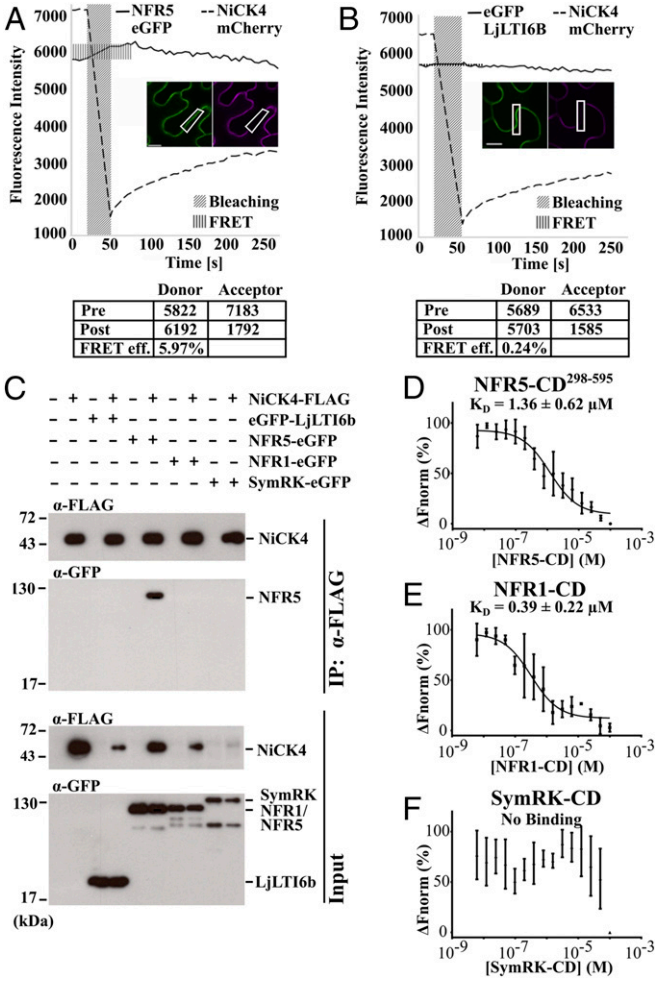

Donor	Acceptor
Pre	5822	7183
Post	6192	1792
FRET eff.	5.97%	

Donor	Acceptor
Pre	5689	6533
Post	5703	1585
FRET eff.	0.24%	

Fig. 2. Binding studies of NiCK4 and NFR5. (*A* and *B*) FRET measurements performed for the NFR5-eGFP/NiCK4-mCherry (*A*) or eGFP-*Lj*LTI6b/NiCK4-mCherry (*B*) pairs in epidermal *N. benthamiana* leaf cells. The bleached regions are outlined by a white box in the corresponding confocal microscopy images. FRET was detected as an increase in GFP fluorescence (marked with vertical lines) after bleaching (marked with diagonal lines) for the NFR5-eGFP/NiCK4-mCherry pair (*A*). No increase in GFP fluorescence after bleaching was observed for the eGFP-*Lj*LTI6b/NiCK4-mCherry pair (*B*). The extracted fluorescence values for donor and acceptor prebleaching/postbleaching and FRET efficiencies are presented in the corresponding tables. (Scale bars: 20 μm.) (*C*) Western blots from anti-FLAG pulldown experiment with *p35S:*NiCK4-FLAG, *p35S:*eGFP-*Lj*LTI6b, *p35S:*NFR5-eGFP, *p35S:*NFR1-eGFP, and *p35S:*SymRK-eGFP expressed in *N. benthamiana*. The eGFP fusion proteins were expressed alone (odd lanes, excluding lane 1 with no transgenic protein) or coexpressed NiCK4-FLAG (even lanes, excluding lane 2). Synthetic FLAG peptide was added to samples containing no transgenic protein or eGFP fusion proteins expressed alone (odd lanes) to prevent unspecific binding of eGFP proteins to the beads and to check for any unspecific binding of the eGFP fusion proteins to the FLAG tag. Crude lysate (Input) and immunoprecipitated (IP) proteins were detected with anti-FLAG or anti-GFP antibodies. The results were reproducible in 3 biological replicates. (*D–F*) MST binding curves obtained from binding experiments with labeled NiCK4 and nonlabeled NFR5-CD$^{298\text{-}595}$, NFR1-CD, or SymRK-CD. NiCK4 directly binds NFR5-CD$^{298\text{-}595}$ (*D*) and NFR1-CD (*E*) but not SymRK-CD (*F*). Binding curves and errors were obtained from 3 biological replicates.

We also investigated whether NiCK4-FLAG associates with NFR1-eGFP and SymRK-eGFP, the proposed coreceptors of NFR5 (6, 13, 21, 22, 63). NFR1-eGFP and SymRK-eGFP were also expressed individually or coexpressed with NiCK4-FLAG in *N. benthamiana* leaves. While no association of NFR1-eGFP or SymRK-eGFP with NiCK4-FLAG was observed in the anti-FLAG pulldown experiments (Fig. 2*C*), we cannot exclude that NFR1-eGFP and SymRK-eGFP were not detected due to lower expression levels compared with NFR5-eGFP (Fig. 2*C*).

Furthermore, we employed the microscale thermophoresis (MST) technique to further investigate whether NiCK4 directly associates with the cytoplasmic domain of NFR5, NFR1, and SymRK. For this purpose, NiCK4, as well as the cytoplasmic domains of NFR5 (NFR5-CD), NFR1 (NFR1-CD), and SymRK (SymRK-CD) were expressed in *Escherichia coli* and purified by affinity and size-exclusion chromatography (SEC) (*SI Appendix*, Fig. S9 *A–C*, and *E*). MST experiments revealed that NiCK4 directly binds NFR5-CD$^{298\text{-}595}$ and NFR1-CD with dissociation constants of 1.36 ± 0.62 μM (Fig. 2*D*) and 0.39 ± 0.22 μM (Fig. 2*E*), respectively, but does not directly bind SymRK-CD (Fig. 2*F*).

NiCK4 Phosphorylates NFR5-CD In Vitro. The cytoplasmic domain of NFR5 contains a degenerated glycine-rich loop and truncated activation loop (Fig. 3*A*), and has consistently been demonstrated to be inactive (7, 12, 13). It has thus remained unclear how the pseudokinase NFR5 contributes to signal initiation following NF perception. Pseudokinases are proposed to act as scaffoldings (64), in which phosphorylation of the pseudokinase domain could potentially result in the formation of docking platforms for downstream signaling components that modulate signaling outputs (65). Unlike NFR5, NiCK4 possesses the hallmark features of an active kinase, such as a glycine-rich loop, the AXK motif, the HRD motif in the catalytic loop, as well as intact DFG and APE motifs in the activation loop (Fig. 3*A*). This, together with our finding that NiCK4 directly interacts with NFR5-CD$^{298\text{-}595}$, led us to investigate whether NiCK4 was an active kinase capable of phosphorylating NFR5-CD. Consistent with previous reports (12, 13), in vitro kinase assays revealed that NFR5-CD does not display any detectable kinase activity (Fig. 3 *B* and *D*, and *SI Appendix*, Figs. S10 and S11*B*). NiCK4, however, is an active kinase capable of autophosphorylation (Fig. 3 *B* and *D*, and *SI Appendix*, Figs. S10 and S11). Remarkably, NiCK4 is also capable of transphosphorylating NFR5-CD$^{298\text{-}595}$ and NFR1-CD-T483A, the kinase-dead variant of NFR1-CD (*SI Appendix*, Fig. S10).

To investigate how the phosphorylation of NFR5 by NiCK4 compares to NFR1 or SymRK, we performed additional in vitro kinase experiments using an extended NFR5-CD$^{276\text{-}595}$ construct that contains all juxtamembrane residues, including the single S282 residue phosphorylated by NFR1-CD (13). Here, NFR1-CD was N-terminally fused to a thioredoxin tag (TRX-NFR1-CD) to facilitate the separation of NFR1-CD and NFR5-CD$^{276\text{-}595}$ on sodium dodecyl sulfate polyacrylamide gel electrophoresis (SDS/PAGE) gels (Fig. 3*B* and *SI Appendix*, Fig. S10). We first determined the conditions in which the kinase activities of NiCK4, TRX-NFR1-CD, and SymRK-CD were optimal by assessing the autophosphorylation abilities of these kinases in buffers containing different divalent metals (Ca^{2+}, Mg^{2+}, Mn^{2+}, and Zn^{2+}) at various concentrations (*SI Appendix*, Fig. S11*A*). As NiCK4 and TRX-NFR1-CD were most active in the presence of 10 mM $MgCl_2$ and SymRK-CD was most active in the presence of 5 mM $MnCl_2$ (*SI Appendix*, Fig. S11*A*), we performed NFR5-CD$^{276\text{-}595}$ phosphorylation studies using a buffer containing 10 mM $MgCl_2$ and 5 mM $MnCl_2$. As observed previously (12, 13), NFR5-CD$^{276\text{-}595}$ lacks kinase activity, and TRX-NFR1-CD, SymRK-CD, and NiCK4 possess both autophosphorylation and transphosphorylation abilities (Fig. 3*B* and *SI Appendix*, Fig. S11). The results from these kinase assays suggest that NiCK4 seems to phosphorylate NFR5-CD$^{276\text{-}595}$ and myelin

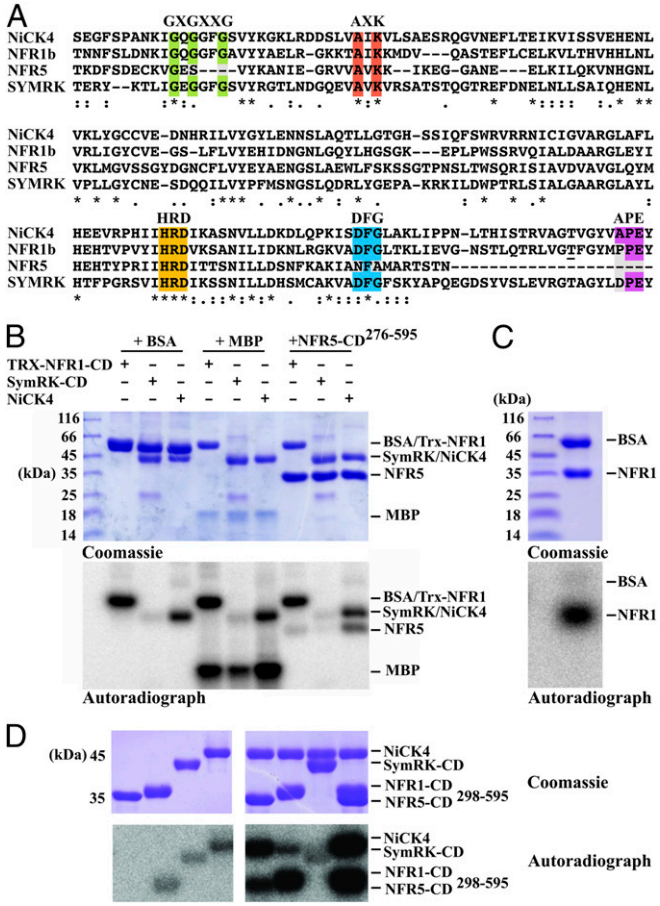

Fig. 3. Kinase activity assessment of NiCK4. (*A*) Amino acid sequence alignment (118) of NiCK4 with the kinase domains of NFR1b, NFR5, and SymRK. NiCK4 possess all features of an active kinase; an intact glycine-rich loop (green) and AXK motif (red); the HRD motif in the catalytic loop (yellow); the DFG motif (blue); and the APE motif in the activation loop (magenta). The threonine residue corresponding to NFR1-CD-T483 is underlined. (*B–D*) SDS/PAGE gels from in vitro kinase assays visualized by Coomassie staining or autoradiography. NiCK4 transphosphorylates myelin basic protein (MBP) and NFR5-CD$^{276-595}$ more strongly than TRX-NFR1-CD or SymRK-CD, but none of the 3 active kinases phosphorylated BSA (*B*). The nonphosphorylation of BSA by TRX-NFR1-CD, which has a similar molecular weight to BSA, was confirmed by NFR-CD lacking the thioredoxin tag (*C*). NFR5-CD$^{298-595}$ and NFR1-CD, but not SymRK-CD were strongly phosphorylated in the presence of NiCK4, while NiCK4 was strongly phosphorylated in the presence of both NFR1-CD and NFR5 (*D*). The phosphorylation results could be reproduced in 3 biological replicates.

basic protein more strongly than TRX-NFR1-CD and SymRK-CD (Fig. 3*B*), but none of the 3 active kinases phosphorylated BSA (Fig. 3 *B* and *C*). All *E. coli*-expressed proteins used in these kinase assays were soluble and nonaggregated as indicated by monodisperse peaks in their SEC profiles (*SI Appendix*, Fig. S9).

Unfortunately, we were unable to assess whether NiCK4 could be phosphorylated by NFR1 or SymRK, as kinase-dead variants of NiCK4 could not be expressed despite numerous attempts. However, NiCK4 is strongly phosphorylated in the presence of both NFR5-CD$^{298-595}$ and kinase-active NFR1-CD but not kinase-active SymRK-CD (Fig. 3*D*). Similarly, NFR5-CD$^{298-595}$ and kinase-active NFR1-CD, but not kinase-active SymRK-CD, are strongly phosphorylated in the presence of NiCK4. It is plausible that NFR5, NFR1, and NiCK4 may form a tripartite signaling complex that serves to amplify the initial NF signal and subsequently activates downstream components involved in symbiosis signaling.

***Nick4* and *Nfr5* Display Similar Expression Patterns.** To dissect the biological relevance of the NiCK4–NFR5 interaction, we first studied the expression profile of *Nick4* and *Nfr5* in *L. japonicus* noninoculated roots or roots inoculated with *M. loti* strain MAFF303099 labeled with dsRed. We used *Nick4* and *Nfr5* promoters to drive the expression of nuclear-localized triple YFP reporter (tYFP-NLS) (66). Expression of these *pNick4*:tYFP-NLS and *pNfr5*:tYFP-NLS constructs were then monitored in *L. japonicus* transformed roots (67–69).

The expression pattern we observed for *pNfr5*:tYFP-NLS is consistent with previous reports (70). In noninoculated roots and inoculated roots, *pNfr5*:tYFP-NLS expression was observed in epidermal cells including root hairs (Fig. 4*B*). Furthermore, the expression of *Nfr5* was present in cortical cells of inoculated roots. The expression of *Nfr5* was strongest in nodule primordia but disappeared in fully developed nodules (Fig. 4*D*). Interestingly, *pNick4*:tYFP-NLS mimics the expression pattern of *pNfr5*:tYFP-NLS. In both noninoculated and inoculated roots, the *pNick4*:tYFP-NLS reporter was expressed in epidermal cells including root hairs (Fig. 4*A*). NiCK4 was also expressed in cortical cells of inoculated roots. Unlike *Nfr5*, however, the expression of *Nick4* was retained in mature nodules, and was predominantly observed in noninfected cells in the nodule parenchyma, nodule epidermis, and outer cortex (71, 72) (Fig. 4*C*).

To investigate whether *Nfr5* and *Nick4* were expressed in the same root hair and nodule cells, *pNick4*:tYFP-NLS and *pNfr5*:mCherry-NLS reporter proteins were coexpressed in *L. japonicus* transformed roots (67–69). The tYFP-NLS reporter was maintained for *pNick4* since the expression of *pNick4*:tYFP-NLS was generally weaker than *pNfr5*:tYFP-NLS. However, *pNfr5*:mCherry-NLS was only detectable after *M. loti* inoculation, with the strongest expression observed in cortical cells. We observed that *pNfr5*:mCherry-NLS and *pNick4*:tYFP-NLS coexpress in the same root hair cells (Fig. 4 *K–M*), cortical cells (Fig. 4 *E–G*), and nodule primordia (Fig. 4 *H–J*). This suggests that NiCK4 and NFR5 may function together from the earliest stages of NF perception to later stages of nodule maturation.

NiCK4 Shuttles from the PM to the Nucleus upon NF Treatment. Intrigued by the observation that the closest *A. thaliana* homolog of NiCK4, *At*CRPK1 (Fig. 1*B* and *SI Appendix*, Fig. S4), relays cold signals from the PM to the nucleus (58), we investigated the localization of NiCK4-eGFP in the susceptible zone of *Lotus* roots before and after treatment with NF. As mentioned previously, NiCK4 localizes to the PM when overexpressed (*SI Appendix*, Fig. S8). Following NF treatment of *pLjUbi*:NiCK4-eGFP transformed wild-type *Lotus* roots, we detected NiCK4-eGFP relocalization to the nucleus in roots hairs of 6 out of 8 roots observed after 90 min of NF treatment (Fig. 5*A*). This NF-induced movement is dependent on both NFR5 and NFR1. No nuclear localization of NiCK4-eGFP was detected in any of the root hairs of 11 *nfr5-2* or 9 *nfr1-1* transformed hairy roots (Fig. 5*A*).

NiCK4 Promotes Nodule Organogenesis but Not Infection Thread Formation. To probe whether NiCK4 was implicated in processes that control nodule organogenesis or infection thread formation, loss-of-function mutants were subsequently obtained from the *Lotus retrotransposon 1* (*LORE1*) mutant resource (73, 74). Three homozygous *LORE1* mutants containing *LORE1* insertions in exonic regions of the *Nick4* gene, named *nick4-1* to *nick4-3*, were isolated for phenotypic analyses (Fig. 5*B*). Plants not containing any *LORE1* insertion from the *nick4-2 LORE1* segregating population were also isolated and served as the wild-type (WT) outsegregant control in these experiments. The WT plant contains an intact *Nick4* gene encoding a 387-aa protein (60). However, insertion of the *LORE1* element in exons 1, 2, and

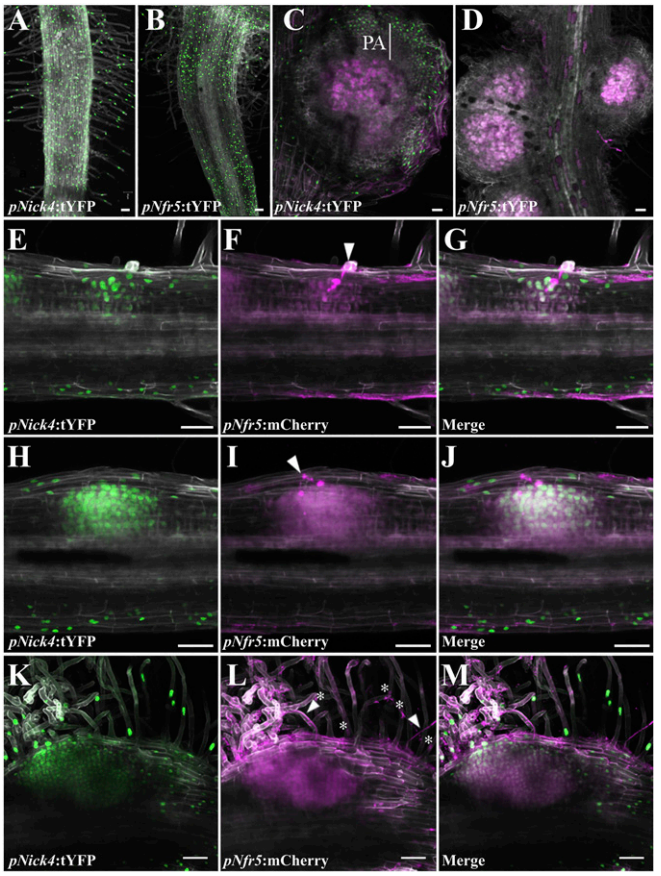

Fig. 4. *NiCK4* and *Nfr5* display similar expression patterns. (*A–D*) Confocal microscopy of *L. japonicus* roots individually expressing *pNick4*:tYFP-NLS (*A* and *C*) or *pNfr5*:tYFP-NLS (*B* and *D*). In noninoculated roots, *pNick4*:tYFP-NLS (*A*) and *pNfr5*:tYFP-NLS (*B*) are expressed in epidermal cells including root hair cells. In nodule primordia, (*C*) *pNick4*:tYFP-NLS expression is maintained in the nodule parenchyma (PA), cortex, and epidermis of mature nodules 14 d postinoculation (dpi) with *M. loti* strain MAFF303099 expressing dsRed. (*D*) The expression of *pNfr5*:tYFP-NLS is strongly down-regulated in mature nodules 14 dpi with *M. loti* strain MAFF303099. (*E–M*) Confocal microscopy of *L. japonicus* roots coexpressing *pNick4*:tYFP-NLS and *pNfr5*:mCherry-NLS. p*Nick4*:tYFP-NLS and *pNfr5*:mCherry-NLS are coexpressed in cortical cells (*E–G*) and nodule primordia (*H–J*) 14 dpi with *M. loti* strain MAFF303099 expressing dsRed. p*Nick4*:tYFP-NLS and *pNfr5*:mCherry-NLS are also coexpressed in root hair cells (*K–M*) 11 dpi with *M. loti* strain MAFF303099. The asterisks (*) indicate root hairs that coexpress *pNfr5*:mCherry-NLS and p*Nick4*:tYFP-NLS. Arrowheads depict infection threads. Autofluorescence, YFP, and mCherry/dsRed channels are represented in white, green, and magenta, respectively. White nuclei indicate merged green and magenta nuclei. (Scale bars: 50 μm.)

4 in the *nick4-1*, *nick4-2*, and *nick4-3* alleles (Fig. 5*B*) introduces frameshift mutations and early stop codons after the sequences that encode K12, G58, and V166, resulting in truncated 18-, 63-, and 201-aa products, respectively (60, 75).

Nick4-1, *nick4-2*, and *nick4-3* mutant plants grown on plates produced significantly fewer nodules ($P < 0.05$) than WT plants 3 wk postinoculation with *M. loti* strain NZP2235 (Fig. 5*C*). Similarly, fewer nodules were observed for *nick4* mutant plants grown in pots in the greenhouse for 8 wk (*SI Appendix*, Fig. S12*A*). There was, however, no significant difference in the number of root hair infection threads formed in WT and mutant plants 10 d postinoculation with *M. loti* strain MAFF303099 (*SI Appendix*, Fig. S12*B*). Altogether, our data suggest NiCK4 as a component downstream of NFR5, which is involved in nodule organogenesis but not infection thread formation.

We hereby propose a model describing NiCK4 as an important signaling component of the NFR5 signaling pathway (Fig. 5*D*). In the presence of NF, NiCK4 phosphorylates NFR5, possibly leading to formation or modification of docking sites for NFR5 interactors including NiCK4 and NFR1. NiCK4 subsequently phosphorylates NFR1, which then phosphorylates and triggers

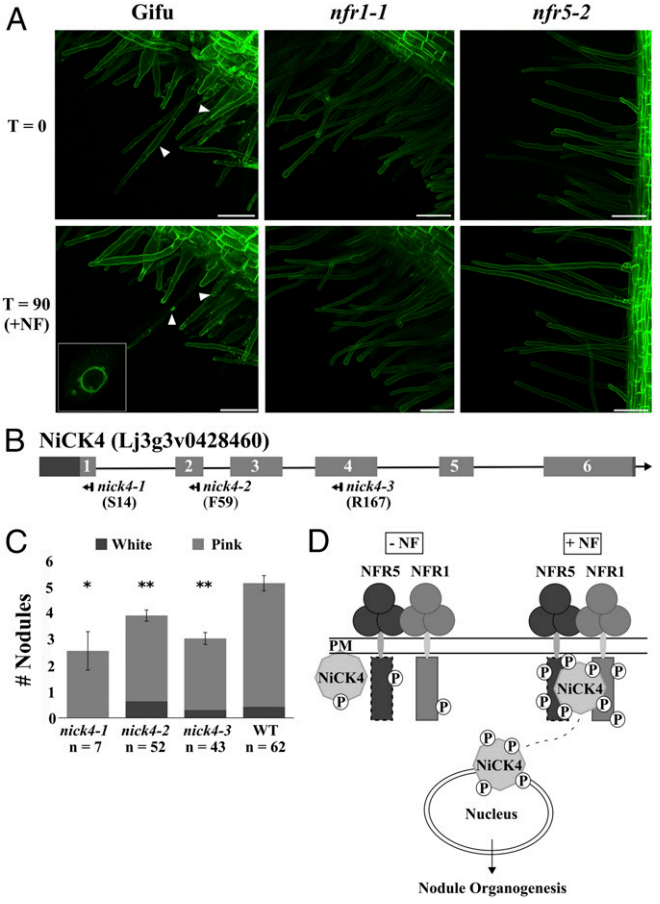

Fig. 5. NiCK4 shuttles to the nucleus after Nod factor (NF) treatment and promotes nodulation. (*A*) In *pLjUbi*:NiCK4-eGFP transformed root systems, NiCK4-eGFP relocates to the nucleus (indicated with arrowheads) 90 min after NF treatment in roots of WT *Lotus* plants but not in transformed *nfr1-1* or *nfr5-2* mutant roots. *Inset* shows nuclear localization of NiCK4-eGFP at higher magnification. T = 0 and T = 90 represent images obtained from the same root hairs before and 90 min after NF treatment, respectively. The number of WT, *nfr5-2*, and *nfr1-1* mutant plants imaged are 8, 11, and 9, respectively. (Scale bars: 50 μm.) (*B*) The predicted gene structure of *Nick4* with six exons indicated. The untranslated regions and coding sequences are represented by filled dark gray and light gray boxes, respectively, and the intronic regions are represented a black line. *LORE1* insertions for *nick4-1*, *nick4-2*, and *nick4-3* alleles before the sequences encoding residues S14, F59, and R127 in exons 1, 2, and 4, respectively, are indicated below the exons. The direction of *LORE1* insertion is indicated by the direction of the arrow. (*C*) Nodulation counts of *nick4* mutants and WT plants grown on agar plates 21 d after inoculation with *M. loti* strain NZP2235. Reduced nodulation was observed in *nick4* mutants compared with WT plants. $*P < 0.05$ and $**P < 0.01$ (*t* test). White and pink nodules are represented by filled dark gray and light gray bars, respectively. (*D*) Working model for NiCK4 involvement in symbiosis signaling. In the presence of NF, NiCK4 phosphorylates NFR5, possibly improving its own docking site(s) or sites for hitherto-unknown NFR5 interactors. NiCK4 then phosphorylates NFR1, which in turn phosphorylates NiCK4 and leads to NiCK4 dissociation and migration to the nucleus. This mechanism would relay the NF signal from the PM-localized receptors to the nuclear components involved in promoting nodule organogenesis. Given the nodulation phenotype of *nick4* mutants, NICK4 is not solely responsible for this relay.

the release of NiCK4 from the tripartite complex. NiCK4, in turn, migrates to the nucleus as one of the signal transduction components that relays the NF signal from PM-localized receptors to nuclear components involved in promoting nodule organogenesis.

Discussion

This study reports a proteomics approach for isolating proteins in the symbiotic receptor complex and the identification of NiCK4 in the nodulation signaling pathway. *Nick4* and *Nfr5* are expressed in the same root hair and cortical cells of *L. japonicus* roots, and the 2 proteins most likely form a complex on the PM as suggested by the FRET analysis in Fig. 2*A*. Upon NF treatment, phosphorylation events in the NFR1–NFR5–NiCK4 tripartite complex result in NiCK4 migrating from the PM to the nucleus. Symbiosis signaling processes that govern nodule organogenesis are then initiated, while the signaling processes required for the formation of root hair infection treads remain unperturbed. Such bifurcation of the signal transduction downstream of NFR1 and NFR5 was previously observed using a genetic dissection of the symbiosis signaling (4). Future work should define how NiCK4 ultimately regulates nodulation. This would involve detailed studies investigating how phosphorylation patterns of NFR5 and NFR1 influence activation of the downstream signal transduction, the role of NiCK4-mediated phosphorylation in this process, and notably the identification of NiCK4 substrates. The reduced nodulation observed in *nick4* mutants indicates that NiCK4 plays a positive role either through modification of NFR5 docking platforms for downstream signaling components or by modification of the NFR1 activity. NiCK4 interaction and phosphorylation of other substrates that may influence signal transduction can also not be excluded.

RLCKs such as *At*CRPK1 and *At*BIK1 have been recently shown to relay signaling from the PM to the nucleus in response to cold or immune signals, respectively (58, 59). Interestingly, NiCK4 also connects NF perception at the PM to nuclear events that lead to nodule organogenesis. NiCK4 and several other NFR5-associated proteins contain closely related family members (Fig. 1*B* and *SI Appendix*, Figs. S3 and S4). This could explain why components downstream of NFR5 have remained elusive in genetic screens and suggest that higher-order mutants may be required to fully uncover their roles in symbiosis signaling.

Perception of extracellular signals in plants commonly involves PM-localized ligand-binding RKs, which typically require 1 (or more) coreceptor(s) and intracellular RLCK(s) (76, 77). The receptor/coreceptor/RLCK signaling mechanism is not limited to LysM-RKs, but is also found in receptor kinases that contain leucine-rich repeats (LRRs) or malectin-like domains (MLDs), as summarized in *SI Appendix*, Fig. S12*C*. In rice [*Oryza sativa* (*Os*)], LysM receptor-like proteins lacking a kinase domain, *Os*CEBIP and *Os*LYP4/LYP6 bind chitin (78) and peptidoglycan (79). The coreceptor *Os*CERK1 and its associated *Os*RLCK185 are essential for downstream chitin- and peptidoglycan-induced immunity signaling (52). In *A. thaliana*, a similar LysM-pseudokinase/LysM-RK/RLCK complex involving *At*LYK5/*At*CERK1/*At*PBL27, respectively, is responsible for chitin-induced MAP kinase activation (80). LRR-RKs such as flg22-binding *At*FLS2 (81) and elf18-binding *At*EFR (82) also require a coreceptor, *At*BAK1 (83), and the RLCK, *At*BIK1, for initiating PAMP-induced reactive oxygen species burst and antibacterial immunity (50, 54). *At*BAK1 is also recruited as a coreceptor for the brassinosteroid (BR) receptor, *At*BRI1 (84–86), which is another LRR-RK that interacts and phosphorylates RLCKs from the BSK family to activate BR signaling (87). Finally, the RALF peptide-binding MLD-containing *At*ANX1/ANX2 receptors most likely work with coreceptors such as other CrRLK1L proteins, *At*BUPS1/BUPS2 (88), or LRR extensin (LRX) proteins (89), as well as the RLCK, *At*MARIS (56), to control pollen tube growth. The identification of NiCK4 as an interactor of NFR5 is therefore in line with these recent discoveries in various signaling processes that illustrate how RLCKs are of paramount importance in mediating signaling downstream of transmembrane receptors (90).

The association of NiCK4 and NFR5 in reciprocal co-IP experiments and the elucidation of the biological role of NiCK4 in promoting nodule organogenesis confirm that our proteomics approach to isolate interactors of NFR5 is valid and technically sound. NFR5-associated proteins with proposed symbiotic functions include *Lj*LNP2 (91–93), *Lj*PLENTY2 (94), and the *L. japonicus* homologs of *Mt*HMGR1 (95, 96), *Mt*SPK1 (97), and *Mt*MCA8 (98). In addition to NiCK4, other interesting interactors that merit functional studies were found.

Three NFR5-associated RKs that were enriched in NF-treated samples include homologs of *A. thaliana* HERK1 CrRLK1L protein that is involved in cell elongation processes (99, 100) and the LRR-RK BIR1 that negatively regulates several plant defense signaling pathways (101, 102), and the *Lj*LYS13 LysM pseudokinase. *Lj*LYS13 is the putative coreceptor of the *Lj*CERK6 chitin receptor (103), which was also identified as an NFR5-associated RK (Table 1). The up-regulation of *Ljlys13* upon treatments/inoculations with *M. loti*, chitin, or *Phytophthora palmivora* (an oomycete plant pathogen) (104, 105) suggests that it could be implicated in symbiotic and defense signaling. Another NF-enriched NFR5-associated protein is the *L. japonicus* homolog of *At*SAL1 that regulates auxin signaling (106) (Table 1). Interestingly, auxin signaling has been proposed to occur in parallel with the common symbiosis signaling pathway as NF-induced auxin accumulation was absent in *nfr1-1* loss-of-function mutants (107).

The 2 NFR5-associated proteins that were found exclusively in mock-treated samples included the *Lj*LNP2 and a B″β regulatory subunit of PP2A (Table 1 and *SI Appendix*, Table S1). *Lj*LNP2 is closely related to *Lj*LNP that has been proposed to function in parallel or downstream of the NF receptors (93). Moreover, PP2A has been shown to negatively regulate RK-mediated immune signaling in plants (108) and could possibly play a similar role in the NF signaling pathway. Other NFR5-associated RKs included a cysteine-rich RK (CRK), another CrRLK1L and *At*BIR1-like protein (101, 102), an *At*RLK7-like protein (109), and a proline-rich extensin-like receptor kinase (PERK) (Table 1 and *SI Appendix*, Fig. S3). Three other RLCKs that associated with NFR5 include homologs of *Mt*SPK1 (97), *At*MARIS (56), and *At*BSK8 (64) (*SI Appendix*, Fig. S4 and Table 1). The PM-localized proton pump, identified as the top NFR5-association protein could explain how depolarization of the PM and alkalization of root hair extracellular space occurs within minutes of NF application (6).

These remaining NFR5-associated proteins should be probed for their roles in symbiosis, defense, or cell wall remodeling. This would allow us to understand how the plant elegantly remodels its cell wall to accommodate rhizobia without mounting full-scale defense responses against them. A greater understanding of the functions of NFR5-associated proteins could also help to shed light on the mechanisms that NFRs use to elicit NF-triggered responses such as perinuclear calcium oscillations, extensive gene activation, root hair deformations, and invagination of the PM and cell wall to form infection threads.

Experimental Procedures

Plant Material and Growth Conditions for IP-MS Experiments. For IP-MS studies, heterozygous T1 Gifu/*p35S*:NFR5-eYFP-HA *Lotus japonicus* transgenic lines were generated by stable transformation of the WT *L. japonicus* Gifu plants (110, 111). WT and T1 seeds were germinated using the sulfuric acid method as previously described (112). Seedlings were grown on 1.4% Agar Noble (Difco) plates, and NFR5-eYFP overexpressing plants were selected by supplementation with 10 μg/mL phosphinothricin and by checking for YFP signal under a DM5500 B fluorescence microscope (Leica). At 8 d post-germination (dpg), WT and selected plants were transferred to 1.4% Agar Noble (Sigma-Aldrich) plates containing quarter-strength B and D media. At 9 dpg, a subset of NFR5-eYFP overexpressing seedlings was assessed for PM localization and response to 200 nM NF using a DM6000 B microscope (Leica). Images were collected at 512–558 nm for YFP using a DAF filter. The plants were incubated at 22 °C under 16-h light and 8-h dark cycle.

Co-IP. At 17 dpg, roots of NFR5-eYFP overexpressing *Lotus* seedlings were individually treated with water (mock) or 200 nM 18:0 NF from *M. loti* strain R7A for 15 min. The roots were harvested and flash frozen in liquid nitrogen. Nontreated WT Gifu plants were used as controls. Root tissues were ground with a mortar and pestle. The samples were further homogenized in a potter tube filled with extraction buffer containing 150 mM Tris·HCl, pH 7.5, 150 mM NaCl, 10 mM EDTA, 10% (vol/vol) glycerol, 10 mM DTT, 1 mM PMSF, P9599 protease inhibitor mixture (Sigma-Aldrich), phosphatase inhibitor mixture 2 (Sigma-Aldrich), phosphatase inhibitor mixture 3 (Sigma-Aldrich), 1.5 mM Na_3VO_4, 1 mM NaF, and 0.5% (wt/vol) PVPP. IGEPAL CA-630 [1.0% (vol/vol)] (Sigma-Aldrich) was added to the extract and the sample was gently agitated at 4 °C for 40 min before centrifugation at 16,000 × *g* at 4 °C. Preequilibrated GFP-Trap beads (ChromoTek) were then added to the supernatant, and the sample was gently agitated for at 4 °C for 2.5 h. The beads were then spun at 100 × *g* for 1 min. The solution was aspirated out, and the beads were washed 3 times with extraction buffer containing 0.5% (instead of 1.0%) IGEPAL CA-630 and no PVPP. Coimmunoprecipitated proteins were eluted by vortexing the samples thoroughly before heating them at 70 °C for 15 min. One microliter of eluted protein samples was separated on an SDS/PAGE gel, and NFR5-eYFP was detected on a film (Fujifilm) via immunoblotting with HRP-conjugated anti-GFP (Santa Cruz) antibodies and using the WB substrate (Pierce ECL). The remaining samples were analyzed on a precast NuPAGE 4–12% Bis-Tris gel (Thermo Fisher Scientific). The gel was stained with SimplyBlue SafeStain (Thermo Fisher Scientific) and excised for MS analysis.

MS. IP-MS analysis of Gifu control and NFR5-eYFP IP samples was done as previously described (113). Gel slices were destained in 50% acetonitrile. Reduction and alkylation was done by incubation for 45 min in 10 mM DTT, followed by 30 min in the dark in 55 mM chloroacetamide. After several washes with 25 mM ammonium bicarbonate, 50% acetonitrile gel slices were dehydrated in 100% acetonitrile. Gel pieces were rehydrated with 50 mM ammonium bicarbonate and 5% acetonitrile containing 20 ng/μL trypsin (Pierce), and digestion proceeded overnight at 37 °C. Tryptic peptides were sonicated from the gel in 5% formic acid and 50% acetonitrile, and the total extracts were evaporated until dry. LC-MS/MS analysis was performed with an Orbitrap Fusion Trihybrid mass spectrometer (Thermo Scientific) and a nanoflow-HPLC system (Dionex Ultimate3000; Thermo Scientific). The peptide identification was performed by searching the *Lotus japonicus* proteome database (version 2.5) using Mascot (version 2.4.1; Matrix Science) with the modification of allowing trypsin peptide termini. Scaffold (version 4; Proteome Software) was used to validate MS/MS-based peptide and protein identifications and to annotate spectra using search criteria of a minimum of 2 peptides with MASCOT ion scores above 20% and 95% peptide identity. Selected spectra were manually inspected before acceptance.

Protein Expression and Imaging in *N. benthamiana* Leaves. The cDNA sequence of the *Nfr1* and *Nfr5*, and genomic sequence of *SymRK*, was available in house, while *Nick4* and *LjLti6b* cDNA sequences were commercially synthesized. These sequences were cloned into the pICH86966 vector using the Golden Gate technology (114) to produce GFP, mCherry, or FLAG fusion constructs. Confocal microscopy images were obtained as described previously (115). Images of *N. benthamiana* epidermal cells were taken 2 d postinoculation with *Agrobacterium tumefaciens* strain GV3101 transformed with plasmid DNA. GFP and mCherry were excited at 488 and 561 nm, respectively. Fluorescence emissions were collected between 500–540 and 590–630 nm for GFP and mCherry, respectively, in separate channels. Reciprocal co-IP studies were performed as previously described (116). FRET measurements were conducted using acceptor photobleaching. Fluorescence emissions were collected between 491–544 and 595–637 nm for GFP (FRET donor) and mCherry (FRET acceptor), respectively, in the same channel with laser power adjusted to avoid acquisition bleaching. Time-lapse images were collected in 5-s intervals in the sequence of five images prior and at least 35 images after photobleaching. No images were captured during the bleaching process. Bleaching parameters were determined empirically to achieve ∼80% decrease in mCherry fluorescence. Fluorescence intensities were extracted from regions of interest using Zeiss ZEN software. FRET efficiency was determined as a percentage difference in mean value of 5 GFP fluorescence intensity measurements after and before photobleaching.

Interaction Studies in *N. benthamiana* Leaves. For reciprocal co-IP experiments with FLAG beads, the procedures were as described above except that the proteins were transiently expressed in *N. benthamiana* and anti-FLAG M2 Affinity Agarose Gel (Sigma-Aldrich) was used. Coimmunoprecipitated proteins were eluted with 100 μg/mL FLAG peptide (Sigma-Aldrich). One hundred micrograms per milliliter FLAG peptide was also added to crude lysates of *N. benthamiana* nontransformed leaves, or leaves expressing NFR5-eGFP or eGFP-*Lj*LTI6b individually to reduce unspecific binding of the eGFP fusion proteins to the anti-FLAG M2 Affinity Agarose Gel in addition to ensuring that the GFP fusion proteins do not unspecifically bind the FLAG-tag.

NiCK4 Expression and Localization in *Lotus* Roots. *pLjUbi*:NiCK4-eGFP with *35S* terminator and *pNick4*:NiCK4-eGFP with *Nick4* terminator expression units were cloned into pIV10 plasmid using Golden Gate cloning system (114). The pIV10-based vectors were conjugated into *Agrobacterium rhizogenes* using triparental mating followed by hairy root induction in *L. japonicus* Gifu as previously described (68, 69). *Lotus* roots expressing *pLjUbi*:NiCK4-eGFP were imaged using 488-nm excitation and 500- to 540-nm emission. Eight WT Gifu, 11 *nfr5-2*, and 9 *nfr1-1* mutant plants were imaged before and 90 min after being treated with 100 nM 18:1 NF from *M. loti* strain R7A.

Protein Expression in *E. coli*. The sequences of *Nick4* and *Symrk-cd* were amplified from *L. japonicus* root cDNA. *Nfr1-cd* and *Nfr5-cd* sequences were amplified from in-house plasmids encoding cDNA sequences of full-length *Nfr1* and *Nfr5*. The sequences were cloned into various vectors to generate *Nick4*, *Nfr1-cd*, *Trx-Nfr1-cd*, *Nfr5-cd*$^{298\text{-}595}$, *Nfr5-cd*$^{276\text{-}595}$, and *Symrk-cd* (*SI Appendix*, Table S5). The single-amino acid substitution for NFR1-T483A was introduced with the QuikChange-Lightning Site-Directed Mutagenesis Kit (Agilent Genomics) using specific primers (*SI Appendix*, Table S6). Sequence-verified plasmids were then transformed into Heat Competent Rosetta 2 *E. coli* cells (Novagen). The protein expression and purification procedures were performed as described in ref. 117. Briefly, the cell pellets were resuspended with lysis buffer containing 50 mM Tris·HCl, pH 8, 500 mM NaCl, 20 mM imidazole, pH 8, 1 mM benzamidine, 5 mM β-mercaptoethanol, and 10% (vol/vol) glycerol. The supernatants were then loaded onto Ni-NTA columns (Qiagen), which were washed with buffer containing 50 mM Tris·HCl, pH 8, 1 M NaCl, 50 mM imidazole, pH 8, 1 mM benzamidine, 5 mM β-mercaptoethanol, and 10% (vol/vol) glycerol. His-tagged proteins were finally eluted with buffer containing 50 mM Tris·HCl, pH 8, 500 mM NaCl, 500 mM imidazole, pH 8, 1 mM benzamidine, 5 mM β-mercaptoethanol, and 10% (vol/vol) glycerol. After TEV protease digestion and a reverse IMAC purification step, the protein samples were loaded onto ENrich 70 10/300 (Bio-Rad), Superdex 75 increase 10/300 (GE Healthcare) or Superdex 200 increase 10/300 (GE Healthcare) SEC columns connected to an ÄKTA PURIFIER system (GE Healthcare). Proteins were eluted with buffer containing 50 mM Tris·HCl, pH 8, 500 mM NaCl, 5 mM β-mercaptoethanol, and 5% (vol/vol) glycerol.

Binding Studies via MST. Protein ligands were dialyzed overnight in buffer containing 50 mM phosphate, pH 7.5, 200 mM NaCl, and 10% glycerol. Proteins to be labeled were first purified on a SEC column and eluted with buffer containing 50 mM phosphate, pH 7.5, 200 mM NaCl, and 5% glycerol before labeling with the Monolith Protein Labeling Kit BLUE (NanoTemper Technologies). Prior to MST measurements, the labeled protein and ligands were spun down at 16,843 × *g* at 4 °C for 30 min to remove aggregated proteins. MST experiments were performed in buffer containing 50 mM phosphate, pH 7.5, 200 mM NaCl, 10% glycerol, 200 μM ATP, pH 7, 4 mM $MgCl_2$, and 0.1% Tween 20. For each MST experiment, a 2-fold dilution series was prepared in which 200 μM of NFR1-CD, NFR5-CD$^{298\text{-}595}$, or SymRK-CD was added to the first tube and titrated 1:1 across the following 15 tubes. An equal volume of 100 to 200 nM labeled NiCK4 protein was then added to all 16 tubes. The proteins were mixed, loaded onto standard glass capillaries (NanoTemper Technologies), and incubated for 1 h at room temperature before analysis on a Monolith NT.115 apparatus (NanoTemper Technologies). MST experiments were run at room temperature with LED powers of 50% or 80%, MST powers of 20% or 50%, 30-s laser on time, and 5-s laser off time. The data were analyzed with the NT-Analysis software (NanoTemper Technologies) and fitted with GraphPad Prism 6 software using the sigmoidal dose–response model to obtain the equilibrium dissociation constant (95% confidence interval).

Phosphorylation Studies. Proteins were incubated with 100 nCi [γ^{32}-P]ATP (PerkinElmer) in 50 mM Tris·HCl, pH 8, buffer containing 10 mM $MgCl_2$, 5 mM $MnCl_2$, and 20 μM cold ATP at room temperature for 1 h. The samples were then separated on SDS/PAGE gels, which were exposed overnight on phosphor plates (Molecular Dynamics). The phosphor plates were scanned with the typhoon TRIO scanner (Amersham Biosciences).

Promoter Studies. Promoter studies were performed as previously described (70). The excitation lasers/emission cutoffs used for confocal microscopy imaging were 405/408–498 nm (autofluorescence), 514/517–550 (YFP), and 561/517–635 nm (dsRed and mCherry). The primers used to amplify the *Nick4* promoter (2,072 bp) are displayed in *SI Appendix*, Table S6.

Phenotyping of *LORE1* Mutants. From segregating *LORE1* population, plants homozygous for the WT gene or *LORE1* insertion in the gene of interest were identified via PCR amplification using gene-specific forward and reverse primers, or the gene-specific forward primer and *LORE1*-specific reverse primer, respectively (*SI Appendix*, Table S6). Homozygous mutants were isolated and assessed for nodulation capacity on 1.4% Agar Noble (Sigma-Aldrich) plates containing quarter-strength B and D media, or in pots containing lightweight expanded clay aggregate (LECA; Saint-Gobain Weber) and vermiculite size M (Damolin). Seedlings were treated with *M. loti* strain NZP2235 (OD_{600} = 0.02) that were grown in yeast mannitol broth at 28 °C for 48 h with a rotational speed of 180 rpm. Plates were incubated at 22 °C under 16-h light and 8-h dark cycle and pots were incubated in the greenhouse. Nodules were counted after 3 and 8 wk, respectively. For infection thread counts, seedlings grown on plates were inoculated with *M. loti* strain MAFF303099 expressing dsRed (OD_{600nm} = 0.01) for 10 d before infection threads were counted.

ACKNOWLEDGMENTS. We thank Anita Bek for performing the NFR5-eYFP complementation experiments in *nfr5*-2 plants, Finn Pedersen for greenhouse assistance, Simon Kelly for providing cDNA from *Lotus* root, Noor de Jong for help with plant transformation, Rikke Jespersen and Dugald Reid for generating and analyzing gene expression data, Hongtao Ji for genotyping *LORE1* mutant plants, and Stig U. Andersen and Peter Roepstorff for scientific discussions. This work was supported by the Danish National Research Foundation Grant DNRF79 (to J.S.), the Gatsby Charitable Foundation and the European Research Council Grant "PHOSPHinnATE" (to C.Z.), a Short-Term Fellowship from the European Molecular Biology Organization (ASTF_615-2014) (to J.E.M.M.W.), and a scholarship (SFRH/BD/79088/2011) from the Portuguese Government (Fundação para a Ciência e a Tecnologia) (to D.C.).

1. R. F. Fisher, S. R. Long, Rhizobium–plant signal exchange. *Nature* **357**, 655–660 (1992).
2. J. Denarie *et al*., "Rhizobium and legume nodulation—a molecular dialog" in *New Horizons in Nitrogen Fixation*. Current Plant Science and Biotechnology in Agriculture, R. Palacios, J. Mora, W. E. Newton, Eds. (Springer, Dordrecht, 1993), vol. 17, pp. 19–30.
3. J. T. Mulligan, S. R. Long, Induction of *Rhizobium meliloti* nodC expression by plant exudate requires nodD. *Proc. Natl. Acad. Sci. U.S.A.* **82**, 6609–6613 (1985).
4. L. H. Madsen *et al*., The molecular network governing nodule organogenesis and infection in the model legume *Lotus japonicus*. *Nat. Commun.* **1**, 10 (2010).
5. E. B. Madsen *et al*., A receptor kinase gene of the LysM type is involved in legume perception of rhizobial signals. *Nature* **425**, 637–640 (2003).
6. S. Radutoiu *et al*., Plant recognition of symbiotic bacteria requires two LysM receptor-like kinases. *Nature* **425**, 585–592 (2003).
7. E. Murakami *et al*., Epidermal LysM receptor ensures robust symbiotic signalling in *Lotus japonicus*. *eLife* **7**, e33506 (2018).
8. P. Lerouge *et al*., Symbiotic host-specificity of *Rhizobium meliloti* is determined by a sulphated and acylated glucosamine oligosaccharide signal. *Nature* **344**, 781–784 (1990).
9. A. S. Bek *et al*., Improved characterization of Nod factors and genetically based variation in LysM receptor domains identify amino acids expendable for Nod factor recognition in *Lotus* spp. *Mol. Plant Microbe Interact.* **23**, 58–66 (2010).
10. S. Kelly, S. Radutoiu, J. Stougaard, Legume LysM receptors mediate symbiotic and pathogenic signalling. *Curr. Opin. Plant Biol.* **39**, 152–158 (2017).
11. C. Zipfel, G. E. Oldroyd, Plant signalling in symbiosis and immunity. *Nature* **543**, 328–336 (2017).
12. A. Broghammer *et al*., Legume receptors perceive the rhizobial lipochitin oligosaccharide signal molecules by direct binding. *Proc. Natl. Acad. Sci. U.S.A.* **109**, 13859–13864 (2012).
13. E. B. Madsen *et al*., Autophosphorylation is essential for the in vivo function of the *Lotus japonicus* Nod factor receptor 1 and receptor-mediated signalling in cooperation with Nod factor receptor 5. *Plant J.* **65**, 404–417 (2011).
14. H. H. Felle *et al*., Nod signal-induced plasma-membrane potential changes in alfalfa root hairs are differentially sensitive to structural modifications of the lipochitooligosaccharide. *Plant J.* **7**, 939–947 (1995).
15. H. H. Felle *et al*., The role of ion fluxes in Nod factor signalling in *Medicago sativa*. *Plant J.* **13**, 455–463 (1998).
16. D. W. Ehrhardt, R. Wais, S. R. Long, Calcium spiking in plant root hairs responding to Rhizobium nodulation signals. *Cell* **85**, 673–681 (1996).
17. S. Niwa *et al*., Responses of a model legume *Lotus japonicus* to lipochitin oligosaccharide nodulation factors purified from *Mesorhizobium loti* JRL501. *Mol. Plant Microbe Interact.* **14**, 848–856 (2001).
18. B. J. Sieberer *et al*., A nuclear-targeted cameleon demonstrates intranuclear Ca^{2+} spiking in *Medicago truncatula* root hairs in response to rhizobial nodulation factors. *Plant Physiol.* **151**, 1197–1206 (2009).
19. L. Schauser *et al*., Symbiotic mutants deficient in nodule establishment identified after T-DNA transformation of *Lotus japonicus*. *Mol. Gen. Genet.* **259**, 414–423 (1998).
20. M. Kawaguchi *et al*., Root, root hair, and symbiotic mutants of the model legume *Lotus japonicus*. *Mol. Plant Microbe Interact.* **15**, 17–26 (2002).
21. M. K. Ried, M. Antolín-Llovera, M. Parniske, Spontaneous symbiotic reprogramming of plant roots triggered by receptor-like kinases. *eLife* **3**, e03891 (2014).
22. S. Radutoiu *et al*., LysM domains mediate lipochitin-oligosaccharide recognition and Nfr genes extend the symbiotic host range. *EMBO J.* **26**, 3923–3935 (2007).
23. G. Endre *et al*., A receptor kinase gene regulating symbiotic nodule development. *Nature* **417**, 962–966 (2002).
24. S. Stracke *et al*., A plant receptor-like kinase required for both bacterial and fungal symbiosis. *Nature* **417**, 959–962 (2002).
25. K. Saito *et al*., NUCLEOPORIN85 is required for calcium spiking, fungal and bacterial symbioses, and seed production in *Lotus japonicus*. *Plant Cell* **19**, 610–624 (2007).
26. N. Kanamori *et al*., A nucleoporin is required for induction of Ca^{2+} spiking in legume nodule development and essential for rhizobial and fungal symbiosis. *Proc. Natl. Acad. Sci. U.S.A.* **103**, 359–364 (2006).
27. M. Groth *et al*., NENA, a *Lotus japonicus* homolog of Sec13, is required for rhizodermal infection by arbuscular mycorrhiza fungi and rhizobia but dispensable for cortical endosymbiotic development. *Plant Cell* **22**, 2509–2526 (2010).
28. J. M. Ané *et al*., *Medicago truncatula* DMI1 required for bacterial and fungal symbioses in legumes. *Science* **303**, 1364–1367 (2004).
29. M. Charpentier *et al*., *Lotus japonicus* CASTOR and POLLUX are ion channels essential for perinuclear calcium spiking in legume root endosymbiosis. *Plant Cell* **20**, 3467–3479 (2008).
30. R. J. Wais *et al*., Genetic analysis of calcium spiking responses in nodulation mutants of *Medicago truncatula*. *Proc. Natl. Acad. Sci. U.S.A.* **97**, 13407–13412 (2000).
31. M. Charpentier *et al*., Nuclear-localized cyclic nucleotide-gated channels mediate symbiotic calcium oscillations. *Science* **352**, 1102–1105 (2016).
32. J. Lévy *et al*., A putative Ca^{2+} and calmodulin-dependent protein kinase required for bacterial and fungal symbioses. *Science* **303**, 1361–1364 (2004).
33. R. M. Mitra *et al*., A Ca^{2+}/calmodulin-dependent protein kinase required for symbiotic nodule development: Gene identification by transcript-based cloning. *Proc. Natl. Acad. Sci. U.S.A.* **101**, 4701–4705 (2004).
34. L. Tirichine *et al*., Deregulation of a Ca^{2+}/calmodulin-dependent kinase leads to spontaneous nodule development. *Nature* **441**, 1153–1156 (2006).
35. K. Yano *et al*., CYCLOPS, a mediator of symbiotic intracellular accommodation. *Proc. Natl. Acad. Sci. U.S.A.* **105**, 20540–20545 (2008).
36. S. Singh, K. Katzer, J. Lambert, M. Cerri, M. Parniske, CYCLOPS, a DNA-binding transcriptional activator, orchestrates symbiotic root nodule development. *Cell Host Microbe* **15**, 139–152 (2014).
37. L. Schauser, A. Roussis, J. Stiller, J. Stougaard, A plant regulator controlling development of symbiotic root nodules. *Nature* **402**, 191–195 (1999).
38. P. Kaló *et al*., Nodulation signaling in legumes requires NSP2, a member of the GRAS family of transcriptional regulators. *Science* **308**, 1786–1789 (2005).
39. P. Smit *et al*., NSP1 of the GRAS protein family is essential for rhizobial Nod factor-induced transcription. *Science* **308**, 1789–1791 (2005).
40. A. B. Heckmann *et al*., *Lotus japonicus* nodulation requires two GRAS domain regulators, one of which is functionally conserved in a non-legume. *Plant Physiol.* **142**, 1739–1750 (2006).
41. Y. Murakami *et al*., Positional cloning identifies *Lotus japonicus* NSP2, a putative transcription factor of the GRAS family, required for NIN and ENOD40 gene expression in nodule initiation. *DNA Res.* **13**, 255–265 (2006).
42. J. F. Marsh *et al*., *Medicago truncatula* NIN is essential for rhizobial-independent nodule organogenesis induced by autoactive calcium/calmodulin-dependent protein kinase. *Plant Physiol.* **144**, 324–335 (2007).
43. T. Soyano, H. Kouchi, A. Hirota, M. Hayashi, Nodule inception directly targets NF-Y subunit genes to regulate essential processes of root nodule development in *Lotus japonicus*. *PLoS Genet.* **9**, e1003352 (2013).
44. M. S. Hossain *et al*., *Lotus japonicus* NF-YA1 plays an essential role during nodule differentiation and targets members of the SHI/STY gene family. *Mol. Plant Microbe Interact.* **29**, 950–964 (2016).
45. Y. Kawaharada, E. K. James, S. Kelly, N. Sandal, J. Stougaard, The ethylene responsive factor required for nodulation 1 (ERN1) transcription factor is required for infection-thread formation in *Lotus japonicus*. *Mol. Plant Microbe Interact.* **30**, 194–204 (2017).
46. Y. Kadota, A. P. Macho, C. Zipfel, Immunoprecipitation of plasma membrane receptor-like kinases for identification of phosphorylation sites and associated proteins. *Methods Mol. Biol.* **1363**, 133–144 (2016).
47. S. C. Mithoe, F. L. H. Menke, Regulation of pattern recognition receptor signalling by phosphorylation and ubiquitination. *Curr. Opin. Plant Biol.* **45**, 162–170 (2018).
48. S. Dam *et al*., Proteome reference maps of the *Lotus japonicus* nodule and root. *Proteomics* **14**, 230–240 (2014).
49. T. W. Kim *et al*., Brassinosteroid signal transduction from cell-surface receptor kinases to nuclear transcription factors. *Nat. Cell Biol.* **11**, 1254–1260 (2009).
50. D. Lu *et al*., A receptor-like cytoplasmic kinase, BIK1, associates with a flagellin receptor complex to initiate plant innate immunity. *Proc. Natl. Acad. Sci. U.S.A.* **107**, 496–501 (2010).

51. H. Shi *et al*., BR-SIGNALING KINASE1 physically associates with FLAGELLIN SENSING2 and regulates plant innate immunity in *Arabidopsis*. *Plant Cell* **25**, 1143–1157 (2013).
52. K. Yamaguchi *et al*., A receptor-like cytoplasmic kinase targeted by a plant pathogen effector is directly phosphorylated by the chitin receptor and mediates rice immunity. *Cell Host Microbe* **13**, 347–357 (2013).
53. Y. Ao *et al*., OsCERK1 and OsRLCK176 play important roles in peptidoglycan and chitin signaling in rice innate immunity. *Plant J.* **80**, 1072–1084 (2014).
54. Y. Kadota *et al*., Direct regulation of the NADPH oxidase RBOHD by the PRR-associated kinase BIK1 during plant immunity. *Mol. Cell* **54**, 43–55 (2014).
55. L. Li *et al*., The FLS2-associated kinase BIK1 directly phosphorylates the NADPH oxidase RbohD to control plant immunity. *Cell Host Microbe* **15**, 329–338 (2014).
56. A. Boisson-Dernier, C. M. Franck, D. S. Lituiev, U. Grossniklaus, Receptor-like cytoplasmic kinase MARIS functions downstream of CrRLK1L-dependent signaling during tip growth. *Proc. Natl. Acad. Sci. U.S.A.* **112**, 12211–12216 (2015).
57. C. Du *et al*., Receptor kinase complex transmits RALF peptide signal to inhibit root growth in *Arabidopsis*. *Proc. Natl. Acad. Sci. U.S.A.* **113**, E8326–E8334 (2016).
58. Z. Liu *et al*., Plasma membrane CRPK1-mediated phosphorylation of 14-3-3 proteins induces their nuclear import to fine-tune CBF signaling during cold response. *Mol. Cell* **66**, 117–128.e5 (2017).
59. N. K. Lal *et al*., The receptor-like cytoplasmic kinase BIK1 localizes to the nucleus and regulates defense hormone expression during plant innate immunity. *Cell Host Microbe* **23**, 485–497.e5 (2018).
60. T. Mun, A. Bachmann, V. Gupta, J. Stougaard, S. U. Andersen, Lotus Base: An integrated information portal for the model legume *Lotus japonicus*. *Sci. Rep.* **6**, 39447 (2016).
61. S. Kelly, T. Mun, J. Stougaard, C. Ben, S. U. Andersen, Distinct *Lotus japonicus* transcriptomic responses to a spectrum of bacteria ranging from symbiotic to pathogenic. *Front. Plant Sci.* **9**, 1218 (2018).
62. T. Suzaki *et al*., Positive and negative regulation of cortical cell division during root nodule development in *Lotus japonicus* is accompanied by auxin response. *Development* **139**, 3997–4006 (2012).
63. M. Antolín-Llovera, M. K. Ried, M. Parniske, Cleavage of the SYMBIOSIS RECEPTOR-LIKE KINASE ectodomain promotes complex formation with Nod factor receptor 5. *Curr. Biol.* **24**, 422–427 (2014).
64. C. Grütter, S. Sreeramulu, G. Sessa, D. Rauh, Structural characterization of the RLCK family member BSK8: A pseudokinase with an unprecedented architecture. *J. Mol. Biol.* **425**, 4455–4467 (2013).
65. B. S. Blaum *et al*., Structure of the pseudokinase domain of BIR2, a regulator of BAK1-mediated immune signaling in *Arabidopsis*. *J. Struct. Biol.* **186**, 112–121 (2014).
66. D. E. Reid, A. B. Heckmann, O. Novák, S. Kelly, J. Stougaard, CYTOKININ OXIDASE/DEHYDROGENASE3 maintains cytokinin homeostasis during root and nodule development in *Lotus japonicus*. *Plant Physiol.* **170**, 1060–1074 (2016).
67. A. Petit *et al*., Transformation and regeneration of the legume *Lotus-corniculatus*—a system for molecular studies of symbiotic nitrogen-fixation. *Mol. Gen. Genet.* **207**, 245–250 (1987).
68. J. Stougaard, D. Abildsten, K. A. Marcker,The *Agrobacterium* rhizogenes pRi TL-DNA segment as a gene vector system for transformation of plant. *Mol. Gen. Genet.* **207**, 251–255 (1987).
69. J. Hansen, J. E. Jørgensen, J. Stougaard, K. A. Marcker, Hairy roots—a short cut to transgenic root nodules. *Plant Cell Rep.* **8**, 12–15 (1989).
70. Y. Kawaharada *et al*., Differential regulation of the Epr3 receptor coordinates membrane-restricted rhizobial colonization of root nodule primordia. *Nat. Commun.* **8**, 14534 (2017).
71. F. C. Guinel, Getting around the legume nodule: I. The structure of the peripheral zone in four nodule types. *Botany* **87**, 1117–1138 (2009).
72. S. Gavrilovic, Z. Yan, A. M. Jurkiewicz, J. Stougaard, K. Markmann, Inoculation insensitive promoters for cell type enriched gene expression in legume roots and nodules. *Plant Methods* **12**, 4 (2016).
73. D. F. Urbański, A. Małolepszy, J. Stougaard, S. U. Andersen, Genome-wide LORE1 retrotransposon mutagenesis and high-throughput insertion detection in *Lotus japonicus*. *Plant J.* **69**, 731–741 (2012).
74. A. Małolepszy *et al*., The LORE1 insertion mutant resource. *Plant J.* **88**, 306–317 (2016).
75. L. H. Madsen *et al*., LORE1, an active low-copy-number TY3-gypsy retrotransposon family in the model legume *Lotus japonicus*. *Plant J.* **44**, 372–381 (2005).
76. D. Couto, C. Zipfel, Regulation of pattern recognition receptor signalling in plants. *Nat. Rev. Immunol.* **16**, 537–552 (2016).
77. U. Hohmann, K. Lau, M. Hothorn, The structural basis of ligand perception and signal activation by receptor kinases. *Annu. Rev. Plant Biol.* **68**, 109–137 (2017).
78. M. Hayafune *et al*., Chitin-induced activation of immune signaling by the rice receptor CEBiP relies on a unique sandwich-type dimerization. *Proc. Natl. Acad. Sci. U.S.A.* **111**, E404–E413 (2014).
79. B. Liu *et al*., Lysin motif-containing proteins LYP4 and LYP6 play dual roles in peptidoglycan and chitin perception in rice innate immunity. *Plant Cell* **24**, 3406–3419 (2012).
80. K. Yamada *et al*., The *Arabidopsis* CERK1-associated kinase PBL27 connects chitin perception to MAPK activation. *EMBO J.* **35**, 2468–2483 (2016).
81. D. Chinchilla, Z. Bauer, M. Regenass, T. Boller, G. Felix, The *Arabidopsis* receptor kinase FLS2 binds flg22 and determines the specificity of flagellin perception. *Plant Cell* **18**, 465–476 (2006).
82. C. Zipfel *et al*., Perception of the bacterial PAMP EF-Tu by the receptor EFR restricts *Agrobacterium*-mediated transformation. *Cell* **125**, 749–760 (2006).
83. D. Chinchilla *et al*., A flagellin-induced complex of the receptor FLS2 and BAK1 initiates plant defence. *Nature* **448**, 497–500 (2007).
84. J. Li *et al*., BAK1, an *Arabidopsis* LRR receptor-like protein kinase, interacts with BRI1 and modulates brassinosteroid signaling. *Cell* **110**, 213–222 (2002).
85. K. H. Nam, J. Li, BRI1/BAK1, a receptor kinase pair mediating brassinosteroid signaling. *Cell* **110**, 203–212 (2002).
86. T. Kinoshita *et al*., Binding of brassinosteroids to the extracellular domain of plant receptor kinase BRI1. *Nature* **433**, 167–171 (2005).
87. W. Tang *et al*., BSKs mediate signal transduction from the receptor kinase BRI1 in *Arabidopsis*. *Science* **321**, 557–560 (2008).
88. Z. Ge *et al*., *Arabidopsis* pollen tube integrity and sperm release are regulated by RALF-mediated signaling. *Science* **358**, 1596–1600 (2017).
89. M. A. Mecchia *et al*., RALF4/19 peptides interact with LRX proteins to control pollen tube growth in *Arabidopsis*. *Science* **358**, 1600–1603 (2017).
90. X. Liang, J. M. Zhou, Receptor-like cytoplasmic kinases: Central players in plant receptor kinase-mediated signaling. *Annu. Rev. Plant Biol.* **69**, 267–299 (2018).
91. M. E. Etzler *et al*., A nod factor binding lectin with apyrase activity from legume roots. *Proc. Natl. Acad. Sci. U.S.A.* **96**, 5856–5861 (1999).
92. M. T. Navarro-Gochicoa, S. Camut, A. Niebel, J. V. Cullimore, Expression of the apyrase-like APY1 genes in roots of *Medicago truncatula* is induced rapidly and transiently by stress and not by *Sinorhizobium meliloti* or Nod factors. *Plant Physiol.* **131**, 1124–1136 (2003).
93. N. J. Roberts *et al*., Rhizobial and mycorrhizal symbioses in *Lotus japonicus* require lectin nucleotide phosphohydrolase, which acts upstream of calcium signaling. *Plant Physiol.* **161**, 556–567 (2013).
94. C. Yoshida, S. Funayama-Noguchi, M. Kawaguchi, Plenty, a novel hypernodulation mutant in *Lotus japonicus*. *Plant Cell Physiol.* **51**, 1425–1435 (2010).
95. Z. Kevei *et al*., 3-hydroxy-3-methylglutaryl coenzyme a reductase 1 interacts with NORK and is crucial for nodulation in *Medicago truncatula*. *Plant Cell* **19**, 3974–3989 (2007).
96. M. Venkateshwaran *et al*., A role for the mevalonate pathway in early plant symbiotic signaling. *Proc. Natl. Acad. Sci. U.S.A.* **112**, 9781–9786 (2015).
97. E. Andrio *et al*., Hydrogen peroxide-regulated genes in the *Medicago truncatula–Sinorhizobium meliloti* symbiosis. *New Phytol.* **198**, 179–189 (2013).
98. W. Capoen *et al*., Nuclear membranes control symbiotic calcium signaling of legumes. *Proc. Natl. Acad. Sci. U.S.A.* **108**, 14348–14353 (2011).
99. H. Guo *et al*., Three related receptor-like kinases are required for optimal cell elongation in *Arabidopsis thaliana*. *Proc. Natl. Acad. Sci. U.S.A.* **106**, 7648–7653 (2009).
100. H. Guo, H. Ye, L. Li, Y. Yin, A family of receptor-like kinases are regulated by BES1 and involved in plant growth in *Arabidopsis thaliana*. *Plant Signal. Behav.* **4**, 784–786 (2009).
101. M. Gao *et al*., Regulation of cell death and innate immunity by two receptor-like kinases in *Arabidopsis*. *Cell Host Microbe* **6**, 34–44 (2009).
102. T. Halter *et al*., The leucine-rich repeat receptor kinase BIR2 is a negative regulator of BAK1 in plant immunity. *Curr. Biol.* **24**, 134–143 (2014).
103. Z. Bozsoki *et al*., Receptor-mediated chitin perception in legume roots is functionally separable from Nod factor perception. *Proc. Natl. Acad. Sci. U.S.A.* **114**, E8118–E8127 (2017).
104. G. V. Lohmann *et al*., Evolution and regulation of the *Lotus japonicus* LysM receptor gene family. *Mol. Plant Microbe Interact.* **23**, 510–521 (2010).
105. W. Fuechtbauer *et al*., LYS12 LysM receptor decelerates *Phytophthora palmivora* disease progression in *Lotus japonicus*. *Plant J.* **93**, 297–310 (2018).
106. M. Dai *et al*., A PP6-type phosphatase holoenzyme directly regulates PIN phosphorylation and auxin efflux in *Arabidopsis*. *Plant Cell* **24**, 2497–2514 (2012).
107. M. Nadzieja, S. Kelly, J. Stougaard, D. Reid, Epidermal auxin biosynthesis facilitates rhizobial infection in *Lotus japonicus*. *Plant J.* **95**, 101–111 (2018).
108. C. Segonzac *et al*., Negative control of BAK1 by protein phosphatase 2A during plant innate immunity. *EMBO J.* **33**, 2069–2079 (2014).
109. S. Hou *et al*., The secreted peptide PIP1 amplifies immunity through receptor-like kinase 7. *PLoS Pathog.* **10**, e1004331 (2014).
110. K. Handberg, J. Stougaard, *Lotus-japonicus*, an autogamous, diploid legume species for classical and molecular-genetics. *Plant J.* **2**, 487–496 (1992).
111. K. Handberg, J. Stiller, T. Thykjær, J. Stougaard, "Transgenic plants: Agrobacterium-mediated transformation of the diploid legume Lotus japonicus" in *Ln: Cell Biology: A Laboratory Handbook* (Academic Press, New York, 1994), pp. 119–127.
112. Y. Kawaharada *et al*., Receptor-mediated exopolysaccharide perception controls bacterial infection. *Nature* **523**, 308–312 (2015).
113. K. W. Bender *et al*., Autophosphorylation-based calcium (Ca^{2+}) sensitivity priming and Ca^{2+}/calmodulin inhibition of *Arabidopsis thaliana* Ca^{2+}-dependent protein kinase 28 (CPK28). *J. Biol. Chem.* **292**, 3988–4002 (2017).
114. E. Weber, R. Gruetzner, S. Werner, C. Engler, S. Marillonnet, Assembly of designer TAL effectors by Golden Gate cloning. *PLoS One* **6**, e19722 (2011).
115. C. A. Bücherl *et al*., Plant immune and growth receptors share common signalling components but localise to distinct plasma membrane nanodomains. *eLife* **6**, e25114 (2017).
116. D. Couto *et al*., The *Arabidopsis* protein phosphatase PP2C38 negatively regulates the central immune kinase BIK1. *PLoS Pathog.* **12**, e1005811 (2016).
117. J. E. Wong *et al*., An intermolecular binding mechanism involving multiple LysM domains mediates carbohydrate recognition by an endopeptidase. *Acta Crystallogr. D Biol. Crystallogr.* **71**, 592–605 (2015).
118. F. Sievers *et al*., Fast, scalable generation of high-quality protein multiple sequence alignments using Clustal Omega. *Mol. Syst. Biol.* **7**, 539 (2011).